MOLECULAR IMAGING AND BIOLOGY

Published Online: 26 September 2009

Mol Imaging Biol (2010) 12:181–191
DOI: 10.1007/s11307-009-0265-5

RESEARCH ARTICLE

[^{11}C]Gefitinib ([^{11}C]Iressa): Radiosynthesis, *In Vitro* Uptake, and *In Vivo* Imaging of Intact Murine Fibrosarcoma

Ming-Rong Zhang,[1] Katsushi Kumata,[1] Akiko Hatori,[1] Nobuhiko Takai,[2] Jun Toyohara,[3] Tomoteru Yamasaki,[1] Kazuhiko Yanamoto,[1] Joji Yui,[1] Kazunori Kawamura,[1] Sachiko Koike,[2] Koichi Ando,[2] Kazutoshi Suzuki[1]

[1]*Department of Molecular Probes, Molecular Imaging Center, National Institute of Radiological Sciences, 4-9-1 Anagawa, Inage-ku, Chiba, Japan*

[2]*Heavy-Ion Radiobiology Research Group, National Institute of Radiological Sciences, 4-9-1 Anagawa, Inage-ku, Chiba, Japan*

[3]*Division of Clinical Neuroscience, Chiba University Center for Forensic Mental Health, 1-8-1 Inohana, Chuo-Ku, Chiba, Japan*

Abstract

Objective: Gefitinib (*N*-(3-chloro-4-fluorophenyl)-7-methoxy-6-[3-(morpholin-4-yl)propoxy]quinazolin-4-amine, Iressa) is an approved anticancer drug. In this study, we labeled gefitinib with carbon-11 and evaluated [^{11}C]gefitinib to explore its specific binding in intact fibrosarcoma (NFSa)-bearing mice.

Methods: [^{11}C]Gefitinib was synthesized by the reaction of desmethyl precursor (**1**) with [^{11}C]CH_3I. *In vitro* uptake of [^{11}C]gefitinib into NFSa, human-A431 epidermoid carcinoma, and Jurkat T cells was determined. Positron emission tomography (PET) imaging using [^{11}C]gefitinib was performed for NFSa-bearing mice.

Results: [^{11}C]Gefitinib accumulated into NFSa cells with 2.1 uptake ratio (UR)/mg protein in cells. Addition of nonradioactive gefitinib decreased uptake in a concentration-dependent manner. [^{11}C]Gefitinib also had high uptake (2.6 UR/mg protein) into epidermal growth factor receptor/tyrosine kinase (EGFR/TK)-rich A431 cells but low uptake (0.2 UR/mg protein) into EGFR/TK-poor Jurkat cells. *In vivo* distribution study on NFSa-bearing mice by the dissection method revealed that [^{11}C]gefitinib specifically accumulated into the tumor. The ratio of radioactivity in tumors to that in blood and muscle as two comparative regions increased from 0.4 to 6.0 and from 0.6 to 5.0 during this experiment (0–60 min), respectively. PET for NFSa-bearing mice produced a clear tumor image, although high radioactivity was distributed throughout the body. Treatment with nonradioactive gefitinib (100 mg/kg) decreased uptake in the tumor. *In vivo* metabolite analysis demonstrated that [^{11}C]gefitinib was stable in the tumor, liver, kidney, and blood.

Conclusion: These results demonstrated the promising potential of [^{11}C]gefitinib to serve as a PET ligand for *in vivo* imaging of NFSa-bearing mice.

Key words: Iressa, Gefitinib, Positron emission tomography, Carbon-11, Carbon-ion radiotherapy, CIRT, Fibrosarcoma

Correspondence to: Ming-Rong Zhang; *e-mail:* zhang@nirs.go.jp

Introduction

The knowledge that tumor cells are different from normal cells in their abnormal signal transduction has prompted cancer researchers to target these differences for cancer diagnosis and therapy. Overexpression of epidermal growth factor receptor/tyrosine kinase (EGFR/TK) had been documented in numerous human cancers of epithelial origin and was found to correlate with resistance to treatment and poor prognosis. Several cancers of epithelial origin, such as those in the lung, breast, and bladder, have relatively high expressions of EGFR [1–3]. The inhibition of EGFR/TK overexpressed in tumors is an attractive tool for cancer therapy [3, 4]. Gefitinib (*N*-(3-chloro-4-fluorophenyl)-7-methoxy-6-[3-(morpholin-4-yl)propoxy]quinazolin-4-amine; Fig. 1) is an approved anticancer drug inhibiting EGFR/TK in tumors [5–8]. Gefitinib has been shown to reversely block EGFR/TK by binding it to the ATP site and thereby inhibiting tumor growth. Due to therapeutic effects of this agent on advanced nonsmall cell lung cancer (NSCLC), gefitinib has been approved in many countries as a clinically useful drug, namely Iressa^{R}. Although side effects, particularly fibrinous pneumonia, are a serious problem for cancer patients, gefitinib has been used for treatment.

Radiotherapy is another powerful approach in anticancer therapy. So far, X-ray computed tomography [9], magnetic resonance imaging [10], and positron emission tomography (PET) [11, 12] have been used to evaluate the effect of radiotherapy [13, 14]. PET is a powerful modality to determine the efficacy of radiotherapy and to monitor the different functions (receptor, sugar metabolism, and nucleic acid synthesis) of tumor cells [15, 16]. In our institute, carbon-ion radiotherapy (CIRT) using a carbon-ion beam was started in 1994, and more than 3,000 patients suffering from malignant diseases, including NSCLC, have been treated by CIRT [17–19]. PET with [^{11}C]methionine has been used to monitor the response of CIRT in patients with bone and soft tissue sarcoma and rectal cancer [20, 21].

In consideration of the pharmacological profile of gefitinib, we assumed that gefitinib as a drug for molecular target should have high and specific uptake into tumor cells, EGFR-rich organs. Moreover, radiotherapy including CIRT may inhibit proliferation of tumor cells, which also likely inhibits overexpression of EGFR in the cells. Thus, we aimed to determine the uptake of gefitinib into tumor for evaluating the therapeutic effect of CIRT against cancer. Here, as the first step of this study, we labeled gefitinib with a positron-emitting radioactive isotope ^{11}C, performed imaging of [^{11}C]gefitinib for tumor-bearing mice, and examined *in vivo* specific binding of [^{11}C]gefitinib in the tumor. Although gefitinib has been labeled with ^{11}C, to our knowledge, biological evaluation with this probe was not reported [22, 23]. ^{18}F-Labeled gefitinib was previously synthesized [24, 25] and the potential of [^{18}F]gefitinib was investigated by PET study, but neither significant tumor uptake nor specific binding was demonstrated [25].

To evaluate [^{11}C]gefitinib *in vitro* and *in vivo* in this study, we used intact murine fibrosarcoma cells and fibrosarcoma-bearing mice. The tumor cells, originally extracted from naturally occurred fibrosarcoma-bearing mice (NFSa), have been preserved and cultivated in our institute for the past two decades [26]. NFSa cells have become standard cells for assessing the effect of CIRT in rodents in our institute [27–29]. A large number of results regarding the effect of CIRT on NFSa-bearing mice have been acquired. Therefore, if *in vivo* specific binding of [^{11}C]gefitinib in NFSa-bearing mice is confirmed, [^{11}C]gefitinib PET could be used to efficiently assess the effect of CIRT in clinical treatment. In this article, we reported (1) radiosynthesis of [^{11}C]gefitinib, (2) *in vitro* uptake into tumor cell lines, (3) biodistribution in NFSa-bearing mice, and (4) metabolite analysis.

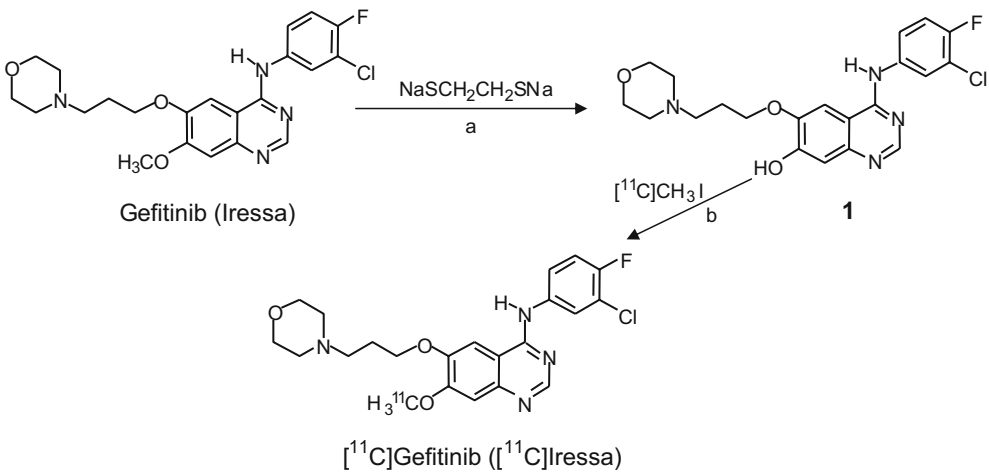

Fig. 1. Chemical synthesis of desmethyl precursor **1** and radiosynthesis of [^{11}C]gefitinib ([^{11}C]Iressa): *a* DMF, 140°C, 3 h; *b* NaH, 70°C, 5 min.

Material and Methods

Chemistry

If not otherwise stated, all chemicals and solvents were purchased from Wako Pure Industries (Osaka, Japan) and Aldrich (Milwaukee, WI, USA) with the highest grade commercially available. Nuclear magnetic resonance (^{1}H-NMR) spectra were recorded on a JNM-GX-300 spectrometer with tetramethylsilane as the internal standard. Fast atom bombardment mass spectra (FAB-MS) were obtained on a JEOL NMS-SX102 spectrometer. Column chromatography was performed on Merck Kieselgel 60 F_{254} (70–230 mesh). Carbon-11 was produced by a ^{14}N(p, α)^{11}C nuclear reaction using a CYPRIS HM-18 cyclotron (Sumitomo Heavy Industry, Tokyo, Japan). A dose calibrator (IGC-3R Curiemeter; Aloka, Tokyo, Japan) was used for all radioactivity measurements if not otherwise stated. Reverse-phase high-performance liquid chromatography (HPLC) was performed using a JASCO HPLC system: Effluent radioactivity was monitored using a NaI (Tl) scintillation detector system.

Chemical Synthesis of N-(3-Chloro-4-fluorophenyl)-7-hydroxy-6-[3-(morpholin-4-yl) propoxy]quinazolin-4-amine (**1**)

Gefitinib (100 mg, 0.22 mmol) was added to a mixture of ethanedithiol (94 μL, 1 mmol) and sodium hydride (88 mg, 2.2 mmol, 60% mineral oil dispersion) in anhydrous dimethylformamide (DMF; 3 mL). This mixture was heated at 140°C for 3 h. After the reaction mixture had cooled, DMF was evaporated under reduced pressure. The reactants were extracted with AcOEt and washed with saturated NH_4Cl three times. After removal of AcOEt, the crude product was purified with silica gel column chromatography using $CHCl_3/CH_3OH$ (100/5) as an eluting solvent to give **1** (58 mg, 65%) as a yellowish crystal. Mp: 116–119°C (Lit. 133–135°C [23]). ^{1}H–NMR (DMSO-d_6) δ: 9.62 (1H, s), 8.55 (1H, s), 8.18 (1H, dd, J= 2.7, 6.9 Hz), 7.82–7.87 (2H, m), 7.50 (1H, t, J=9.0 Hz), 4.24 (2H, t, J=6.3 Hz), 4.00 (3H, s), 3.64 (4H, t, J=4.5 Hz), 2.46 (4H, m), 2.06 (2H, t, J=6.6 Hz). FAB-MS (*m/z*) $C_{21}H_{22}ClFN_4O_3$: 433 (M^++1), 435 (M^++3). For radiosynthesis, the obtained precursor **1** was further purified by semipreparative HPLC.

Radiosynthesis of [^{11}C]Gefitinib

[^{11}C]CH_3I for radiosynthesis was produced from cyclotron-produced [^{11}C]CO_2 as described previously [30]. Briefly, [^{11}C]CO_2 was bubbled into 40 mM $LiAlH_4$ in anhydrous THF (500 μL). After removing THF, the remaining complexes were treated with 57% HI (300 μL). [^{11}C]CH_3I was transferred under helium gas flow with heating into a reactor containing the desmethyl precursor **1** (0.4–0.7 mg) and NaH (10 μL, 0.5 g/20 mL DMF) in anhydrous DMF (300 μL), cooled to −15 to −20°C. After the radioactivity reached a plateau, the reactor was warmed to 70°C and maintained for 5 min. The reaction mixture was applied to a semipreparative HPLC system. HPLC purification was performed on a CAPCELL PAK C_{18} column (10 mm ID×250 mm) using a mobile phase of $CH_3OH/H_2O/Et_3N$ (750/250/1) at a flow rate of 4.0 mL/min. The radioactive fraction of [^{11}C]gefitinib (retention time, 9.5 min) was collected, evaporated, redissolved in 7 mL of normal sterile saline, and passed through a 0.22-μm Millipore filter for analysis and animal experiments.

Radiochemical purity of [^{11}C]gefitinib was assayed by analytical HPLC: CAPCELL PAK C_{18} column (4.6 mm ID×250 mm), $CH_3OH/H_2O/Et_3N$ (750/250/1), 10.2 min, and 1.0 mL/min. The identity of [^{11}C]gefitinib was confirmed by co-injection with an authentic sample. Specific activity of [^{11}C]gefitinib was calculated by comparison of the assayed radioactivity to the mass associated with the carrier UV peak at 254 nm. The mass (micromoles) was determined by HPLC comparison of UV absorbance with those of known concentrations of the corresponding nonradioactive gefitinib.

Evaluation

Animal experiments were carried out according to the recommendations of the Committee for the Care and Use of Laboratory Animals, National Institute of Radiological Sciences.

NFSa Cells and the NFSa-Bearing Mice

C3H/HeMsNrsf male aged 6 to 7 weeks old were produced and maintained in specific pathogen-free facilities in our institute. The tumor was a syngeneic NFSa preserved in our institute, and its 16th generations were implanted subcutaneously with 10^6 cells to the right hind legs of mice. The *in vivo* experiment using NFSa-bearing mice were performed on day 7–10 after implantation of when the tumor was 7–8 mm in diameter.

When tumor had grown to 15 mm in diameter, the mice (n=3) were sacrificed by cervical dislocation. The tumors were removed and minced carefully with surgical scissors. Single-cell suspensions were prepared by enzymatically digesting tumors. NFSa cells were adjusted to 2×10^5 cells/0.5 mL/sample using Hanks solution with 10% fetal bovine serum (FBS) and then used for *in vitro* experiment within 1 h.

A431 and Jurkat Cells

A431 and Jurkat cell lines were obtained from RIKEN BioResource Center (Tsukuba, Japan). The A431 human cell line (EGFR-rich epidermoid carcinoma cell line) was grown in Dulbecco's modified Eagle's medium (DMEM) supplemented with 10% FBS and 1% penicillin and streptomycin at 37°C in 5% CO_2. Similar growth conditions were maintained for the Jurkat cell line (All T-cell line, human EGFR poor), except for the replacement of DMEM with RPMI 1640. A431 cells of 10^5 cells/mL/sample were incubated in 24-well plates for 48 h and then used for the *in vitro* experiment. After a sufficient number of Jurkat cells were grown in culture, cells were adjusted to 2×10^5 cells/0.5 mL/sample for *in vitro* experiment.

In Vitro Uptake into Tumor Cells

NFSa, A431, and Jurkat cells were prepared under each condition described above. To determine the specific binding of [^{11}C] gefitinib, it was added to four different concentrations of non-radioactive gefitinib solutions dissolved in each cell culture medium and preincubated at 37°C. The reaction was initiated by the addition of [^{11}C]gefitinib solutions (3 MBq/sample) to the

incubation chambers for NFSa, A431, and Jurkat cells, respectively, to reach the final concentration of control (no carrier added), 1, 10, and 66 μM. At the designated time points (1, 5, 15, 30, and 60 min), the incubation mixtures of NFSa and Jurkat cells were cooled in an ice bath to stop the reaction. Cell pellets were obtained by centrifugation and washed three times with ice-cooled phosphate buffered saline. A431 cells were incubated in medium in 24-well plates for the designed times, and then cells were washed and dissolved in 0.2 N NaOH. Radioactivity in the cells was measured using a 1480 Wizard gamma counter (PerkinElmer Japan; Yokohama, Japan). After the radioactivity had decayed, the cell pellet was dissolved in 0.2 N NaOH solution (0.2 mL), and the protein content in the cells was measured using the Lowry method (Bio-Rad, DC Protein Assay; Hercules, CA, USA). Radioactivity in the cell pellet was expressed as an uptake ratio (UP) to that in the incubation mixture per milligrams of protein.

Biodistribution

A solution of [^{11}C]gefitinib (average dose 15 MBq/200 μL; specific activity, 110 GBq/μmol) was injected into NFSa-bearing mice (n=4) *via* the lateral tail vein. The mice were sacrificed by cervical dislocation 1, 5, 15, 30, or 60 min after injection. Blood, brain, liver, lung, heart, kidney, spleen, stomach, small intestine, muscle, and tumor samples were removed quickly. All samples were weighed, and their radioactivity was measured using a gamma counter and expressed as a percentage of the injected dose per gram of wet tissue (% ID/g). All radioactivity measurements were corrected for decay.

Small-Animal PET

PET scans of NFSa-bearing mice were performed using a microPET Focus 220 animal scanner (Siemens Medical Solutions USA; Knoxville, TX, USA) designed for rodents and small monkeys, which provides a 25.8 (transaxial)×7.6-cm^2 (axial) field of view and a spatial resolution of 1.3 mm full width at half maximum at the center of the field of view. Prior to the scans, the mice were anesthetized with 1.5–2% isoflurane in air (flow rate, 2 mL/min). After transmission scans for attenuation correction using a ^{68}Ge–^{68}Ga point source, emission scans were acquired for 60 min in a 3D list mode with an energy window of 350–750 keV, immediately after probe injection. All listed-mode data were sorted in 3D sinograms, which were then Fourier rebinned into 2D sinograms (frames, 20.1 and 20.5 min). Images were reconstructed using 2D-filtered back-projection with a 0.5-mm Hanning filter. A solution of [^{11}C]gefitinib (average dose 15 MBq, 100 GBq/μmol) was injected into NFSa-bearing mice (n=3), and time-sequential tomographic scanning was carried out on transverse and coronary sections of the tumor for 60 min. In carrier-added experiments, a mixture of nonradioactive gefitinib (1, 10, or 100 mg/kg) with [^{11}C]gefitinib (15 MBq, 85 GBq/μmol) was injected into NFSa-bearing mice (n=3/dose). Time–activity curves (TACs) in the tumor and muscle were obtained for each scan. These experiments were performed three times using different mice.

Metabolite Analysis

After injection of [^{11}C]gefitinib (37 MBq/200–300 μL) into NFSa-bearing mice (n=3), the mice were sacrificed by cervical dislocation at 60 min, and blood, tumor, liver, and kidney samples were obtained quickly. The blood sample (500 μL) was centrifuged at 15,000 rpm for 2 min at 4°C to separate plasma, which (250 μL) was collected in a test tube containing CH_3CN (500 μL) and gefitinib (10 μL, 0.8 mg/5 mL of CH_3CN). The tube was vortexed for 15 s for deproteinization and centrifuged at 15,000 rpm for 2 min, and the supernatant was collected for HPLC analysis. The other sample (0.5–1.0 g) was homogenized in an ice-cooled CH_3CN/H_2O (1/1, 2 mL) solution containing gefitinib. The produced homogenate was centrifuged at 15,000 rpm for 3 min at 4°C and the supernatant was collected.

An aliquot of the supernatant (100–500 μL) prepared from the above sample was applied to the HPLC analytic system with a highly sensitive positron detector [31] to monitor radioactivity. The HPLC condition was identical to that for the determination of radiochemical purity. The percent ratio of [^{11}C]gefitinib to total radioactivity (corrected for decay) on the HPLC chromatogram was calculated as

$$\% = (\textit{peak area for } [^{11}C]\ \textit{gefitinib}/\textit{total peak area}) \times 100.$$

Results

Radiosynthesis

For radiosynthesis, phenol precursor **1** was synthesized by desmethylation of commercially available gefitinib (Fig. 1). Trimethylsilyl iodide, boron tribromide, sodium ethanethiolate, or sodium ethanethiolate/sodium sulfite was tested to remove the methyl group, but no desired product was obtained. Using sodium ethanedithiolate, **1** was obtained with a chemical yield of 65%. In the present study, to completely remove traces of gefitinib, a contamination source which would lower the specific activity of [^{11}C]gefitinib, **1** was further purified by semipreparative HPLC.

Radiosynthesis of [^{11}C]gefitinib was carried out using an automated synthesis system for ^{11}C-labeled radiopharmaceuticals [30]. [^{11}C]Methylation of **1** with [^{11}C]CH_3I was performed in the presence of NaH at 70°C for 5 min. After the reaction, purification, and formulation, [^{11}C]gefitinib was obtained with radioactivity incorporation yields of 41–62% (based on the HPLC purification chromatogram, n=20). Radiosyntheses were completed with an average synthesis time of 23 min from the end of bombardment. At the end of synthesis, [^{11}C]gefitinib of 800–1,100 MBq was obtained as an injectable solution of sterile normal saline after 20 min proton (14.2 MeV on target) bombardment at a beam current of 15 μA (total radioactivity, 22–25 GBq). The decay-corrected radiochemical yield was 11±7% based on the total [^{11}C]CO_2. The final product was radiochemically pure (≥98%) as measured by analytic HPLC with specific activity of 105±44 GBq/μmol at EOS. This product was stable with >95% radiochemical purity after being maintained for 180 min at 25°C.

In Vitro Uptake of [^{11}C]Gefitinib into NFSa, A431, and Jurkat Cells

Fig. 2 shows the *in vitro* uptakes of [^{11}C]gefitinib into NFSa (a), A431 (b), and Jurkat (c) cell lines. When exposed to NFSa cells, [^{11}C]gefitinib showed high initial uptake into the

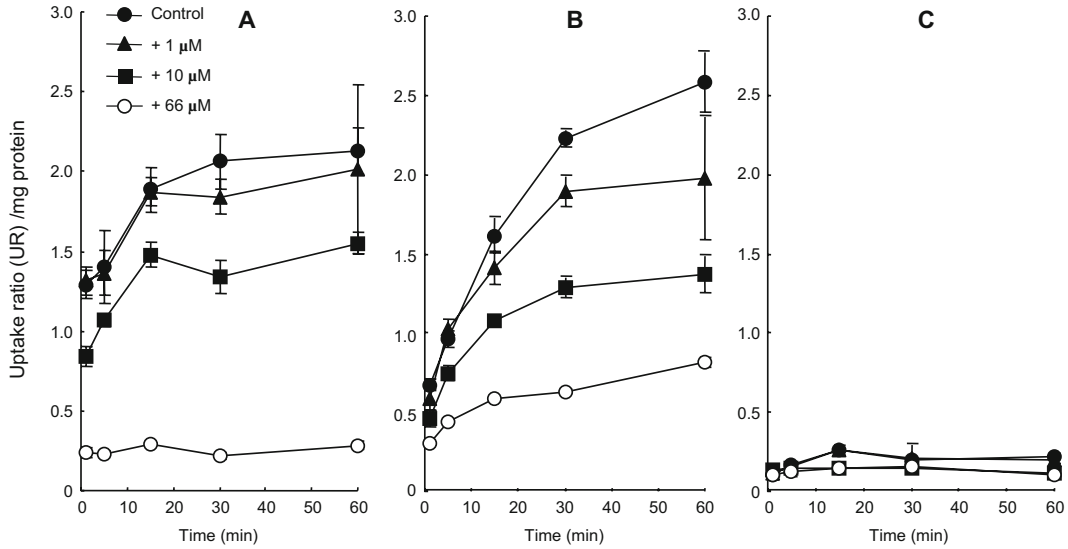

Fig. 2. *In vitro* uptake (uptake ratio/mg protein in cell) of [^{11}C]gefitinib into three tumor cell lines. **a** NFSa cells; **b** EGFR/TK-rich A431 cells; **c** EGFR/TK-poor Jurkat cells. [^{11}C]Gefitinib showed high uptake into NFSa cells. Addition of nonradioactive gefitinib decreased the uptake of [^{11}C]gefitinib in a dose-dependent manner. In EGFR/TK-rich A431 cells, [^{11}C]gefitinib also showed gradual accumulation. In contrast to A431, [^{11}C]gefitinib did not have evident uptake into EGFR/TK-poor Jurkat cells during incubation.

cell, which increased rapidly over time until 15 min after incubation. From 15 min, [^{11}C]gefitinib accumulated gradually to the maximum uptake value of 2.1 UR/mg protein at 60 min. Addition of nonradioactive gefitinib reduced the uptake of [^{11}C]gefitinib in a dose-dependent order. When gefitinib of 66 μM was added to the incubation mixture, the radioactivity level at 60 min decreased to less than 20% of the control. In EGFR/TK-rich A431 cells, [^{11}C]gefitinib also showed gradual accumulation. Radioactivity peaked 2.6 UR/mg protein at 60 min after incubation. Treatment with gefitinib reduced uptake in A431 cells in a dose-dependent order. In contrast to A431, [^{11}C]gefitinib had no evident uptake in EGFR/TK-poor Jurkat cells (<0.2 UR/mg protein) during incubation. Moreover, addition of gefitinib did not change the uptake of [^{11}C]gefitinib.

Biodistribution of [^{11}C]Gefitinib in NFSa-Bearing Mice

Before examining *in vivo* distribution in NFSa-bearing mice, we evaluated the growth of tumors after implantation to determine the optimal experimental period. Fig. 3 shows the radioactivity concentration (% ID/g) in the tumor 7, 14, 21, and 28 days after implantation into the right legs of mice. At the corresponding time points, the average diameters of the tumors were 6, 10, 15, and 18 mm, respectively. During days 7–14 after implantation, the radioactivity of [^{11}C]gefitinib in the tumor was 3.5–2.6% ID/g at 60 min. During days 21–28, the concentration in the tumor decreased to less than 1.5% ID/g while the tumor volume increased significantly. To obtain the highest radioactivity concentration in the tumors, we performed *in vivo* experiments during days 7–10 of tumor growth after implantation.

Fig. 4 shows the distribution data of [^{11}C]gefitinib in the main regions of NFSa-bearing tumors (n=4). High initial radioactivity (>5% ID/g) was found in the lung, heart, liver, and kidney. The lung displayed the highest initial uptake, in agreement with the use of gefitinib as clinical therapy for advanced NSCLC [7]. Radioactivity in the lung and heart subsequently declined rapidly until 5 min and then displayed a slow decrease until the end of the experiment. Compared with the heart and lung, the liver and kidney maintained high concentrations during this experiment. The hepatobiliary, urinary excretion, and intestinal reuptake pathway dominated the whole-body distribution of [^{11}C]gefitinib. Radioactivity gradually accumulated in the small and large intestines. In particular, radioactivity in the small intestine reached 30% ID/g at 60 min after injection. On the other hand, the brain had very low uptake (<0.3% ID/g), suggesting that the drug could not enter the brain easily and may therefore not produce serious side effects in the brain. The main reason for the low concentration in the brain may be that gefitinib is a substrate of the ABCG2 multidrug transporter [32], which could restrict its uptake into the brain from passing through the blood–brain barrier.

[^{11}C]Gefitinib showed rapid uptake (1.6% ID/g) into the tumor at 1 min after injection. Radioactivity in the tumor increased over time and peaked (3.5% ID/g) at 60 min, whereas radioactivity in the blood and muscle as two comparative regions decreased slowly after rapid initial decline. Fig. 5 shows the ratio of radioactivity in the tumor to that in the muscle and blood. The ratios of tumor/muscle at 1, 5, 15, 30, and 60 min were 0.6, 1.5, 2.1, 3.7, and 5.0, while the ratios of tumor/blood were 0.4, 1.5, 2.0, 3.1, and 6.0, respectively.

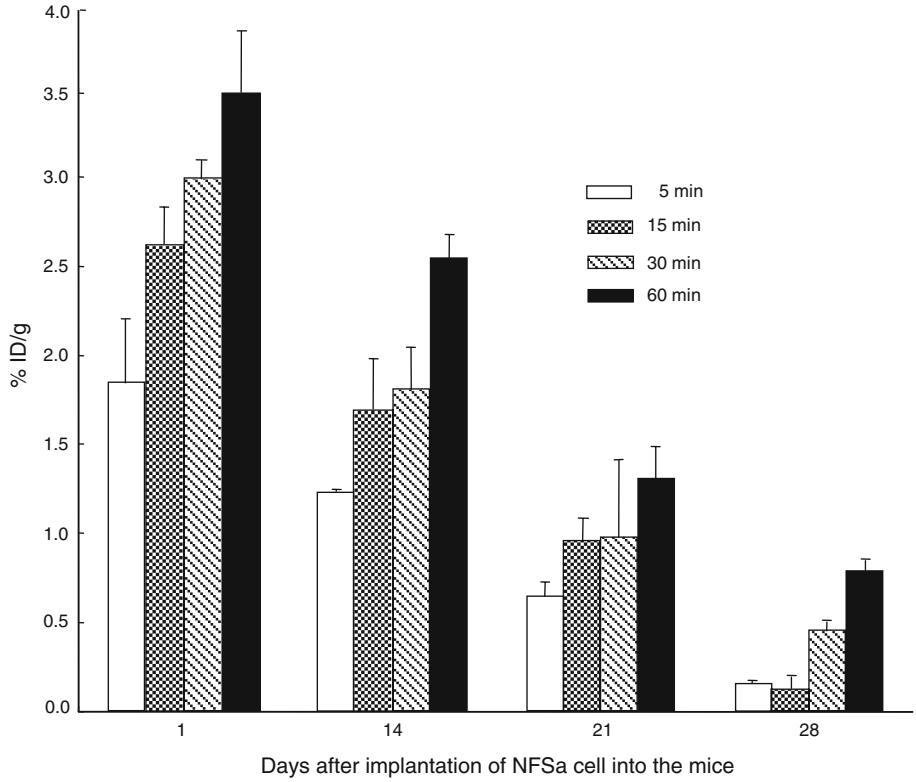

Fig. 3. Radioactivity (mean ± s.d., $n=3$) in tumors after injection of [^{11}C]gefitinib. Tumor samples were obtained from the NFSa-bearing mice at days 7, 14, 21, and 28 after NFSa cells were implanted. During days 7–14 after implantation, the radioactivity of [^{11}C]gefitinib in the tumor was higher than that during days 21–28. To obtain the highest radioactivity concentration in tumors, the present *in vivo* experiments were performed during days 7–10 of tumor growth after implantation.

Small-Animal PET Imaging

Fig. 6 shows the PET result of [^{11}C]gefitinib for NFSa-bearing mice ($n=3$). A typical PET summation image (a and b) acquired from 0 to 60 min after injection displayed evident uptake in the tumor, despite high uptake in the liver, kidney, and gastrointestinal (GI) organs. The time–activity curve (*C*) reflected the gradual accumulation of radioactivity into the tumor (right leg) and a slow decline in the muscle (left leg). The radioactivity ratio of tumor/muscle at 60 min was 2.3±0.2 ($n=3$).

Figs. 7 and 8 show the inhibitory effect of nonradioactive gefitinib on the uptake of [^{11}C]gefitinib in NFSa-bearing mice ($n=3$). As shown in Fig. 7, four PET images (a–d) revealed that co-injection of gefitinib (1, 10, and 100 mg/kg) with [^{11}C]gefitinib reduced the uptake of [^{11}C]gefitinib in the tumor region of same size with a dose-dependent order. By treatment with gefitinib (100 mg/kg), typical summation images (a and b) showed that the difference of radioactivity between the tumor and muscle was almost abolished (Fig. 8). The radioactivity ratio of tumor/muscle was quantified as 1.1±0.2 ($n=3$) from PET images. As shown in the TACs of tumors (Fig. 8c), the control uptake of [^{11}C] gefitinib was decreased to 50% by gefitinib at 60 min after injection.

Metabolite Analysis

Metabolite analysis was performed for plasma, liver, kidney, and tumor samples, which were obtained from mice ($n=3$) 60 min after [^{11}C]gefitinib injection. CH_3CN proved efficient to extract radioactivity and deproteination, and the recovery efficiency into the supernatants was 78–92% of the total radioactivity in the tissues. In all samples, the intact [^{11}C]gefitinib comprised 86.2±1.5% (plasma), 87.9±2.0% (liver), 90.1±1.2% (kidney), and 94.5±2.8% (tumor) of the total radioactivity. Only a tiny fraction corresponded to the radio-labeled metabolites in these samples.

Discussion

In this study, we determined the specific binding of [^{11}C] gefitinib in intact murine fibrosarcoma (NFSa)-bearing mice. So far, many EGFR/TK inhibitors have been developed and labeled using positron- and single photon-emitting radioactive isotopes [33–35]. Although these compounds displayed *in vitro* potent and selective affinity for EGFR/TK, no successful imaging probe was used for clinical investigation. Guaranteed by the reliable effect of gefitinib for the clinical treatment as a drug for molecular target, ^{11}C- or ^{18}F-labeled gefitinib has been developed for PET study without

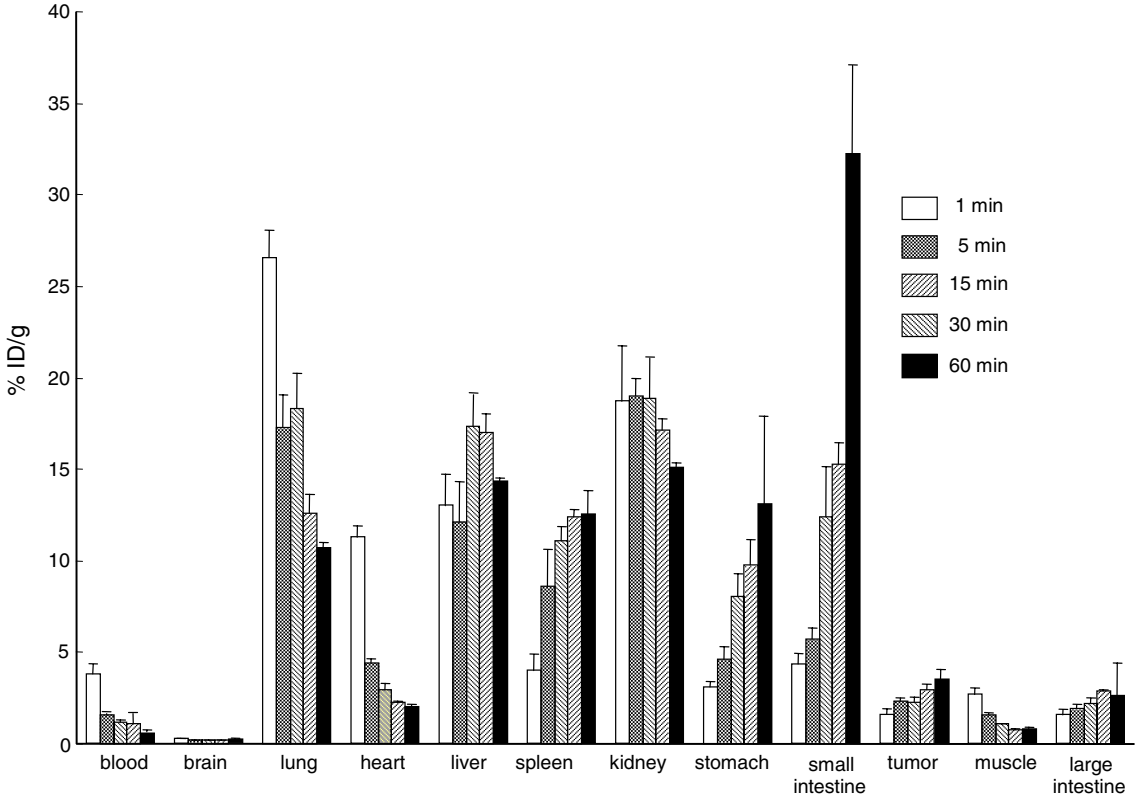

Fig. 4. Biodistribution (mean ± s.d., n=4) in the NFSa-bearing mice after injection of [^{11}C]gefitinib. High initial radioactivity was found in the lung and heart. The liver and kidney maintained high radioactivity levels. Radioactivity gradually accumulated in the small and large intestines. Uptake in the tumor increased over time, whereas those in the blood and muscle declined over time.

changing the chemical structure and pharmacological profile [22–25]. However, despite the radiosynthesis, no biological evaluation with [^{11}C]gefitinib was reported. [^{18}F]Gefitinib was evaluated for the assessment of EGFR status in malignant tumors. However, uptake levels of [^{18}F]gefitinib, both *in vivo* and *in vitro*, did not correlate with EGFR expression levels or the functional status, which was due to the high nonspecific and nonsaturable cellular uptake of gefitinib [25].

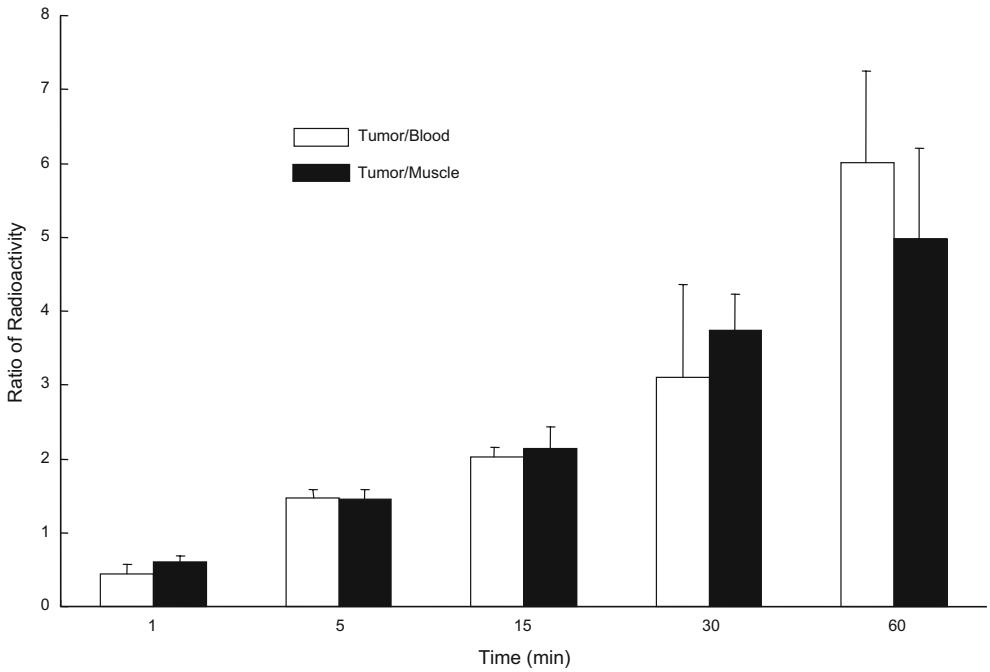

Fig. 5. Ratios of radioactivity in tumor to that in blood or in muscle in the NFSa-bearing mice after injection of [^{11}C]gefitinib. The ratios of tumor/muscle and tumor/blood increased over time.

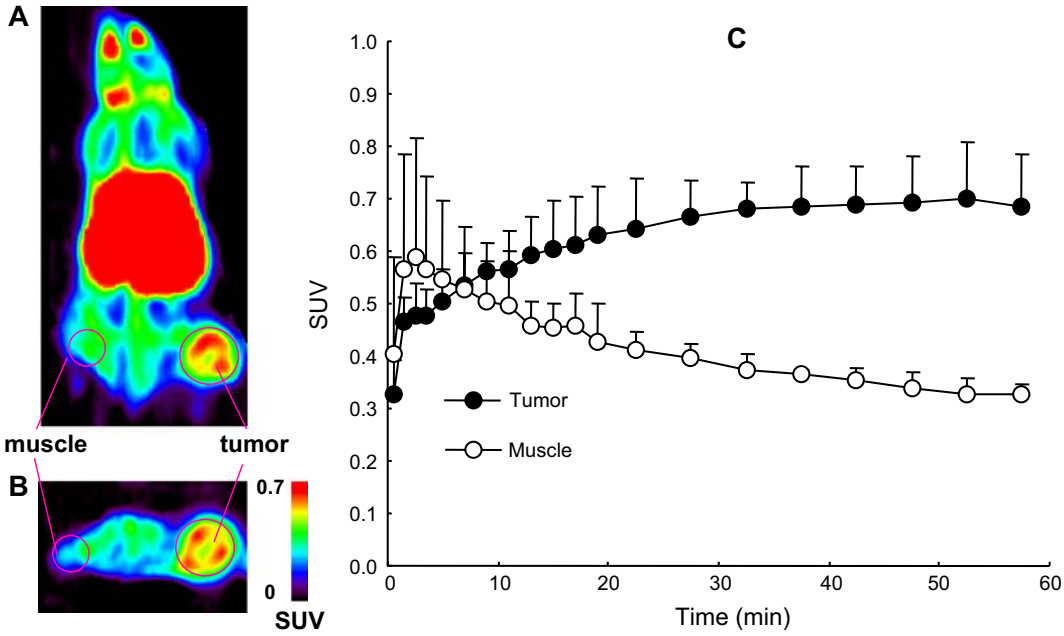

Fig. 6. PET summation images (0–60 min) and time–activity curves of the NFSa-bearing mice. **a** Transverse section; **b** coronary section; **c** TACs ($n=3$) in the tumor (*black dots*) and muscle (*circles*). A typical summation image (**a**, **b**) displayed evident uptake in the tumor, despite high radioactivity in the liver, kidney, and GI organs. TACs reflected the gradual accumulation of radioactivity into the tumor (*right leg*) and slow decline in the muscle (*left leg*). The radioactivity ratio of tumor/muscle at 60 min was 2.3±0.2 ($n=3$).

Since 2002, we have independently synthesized [^{11}C]gefitinib and evaluated this probe using NFSa-bearing mice. In our institute, CIRT has been used to treat patients with various cancers such as bone and soft tissue sarcoma, rectal cancer, and NSLC [17–19]. Our aim was to apply [^{11}C]gefitinib PET to evaluate the effect of CIRT in clinical treatment. As the first step, we explored the specific binding of [^{11}C]gefitinib in NFSa-bearing mice, a standard mouse which has been used to assess the effect of CIRT in our institute for two decades [26–28].

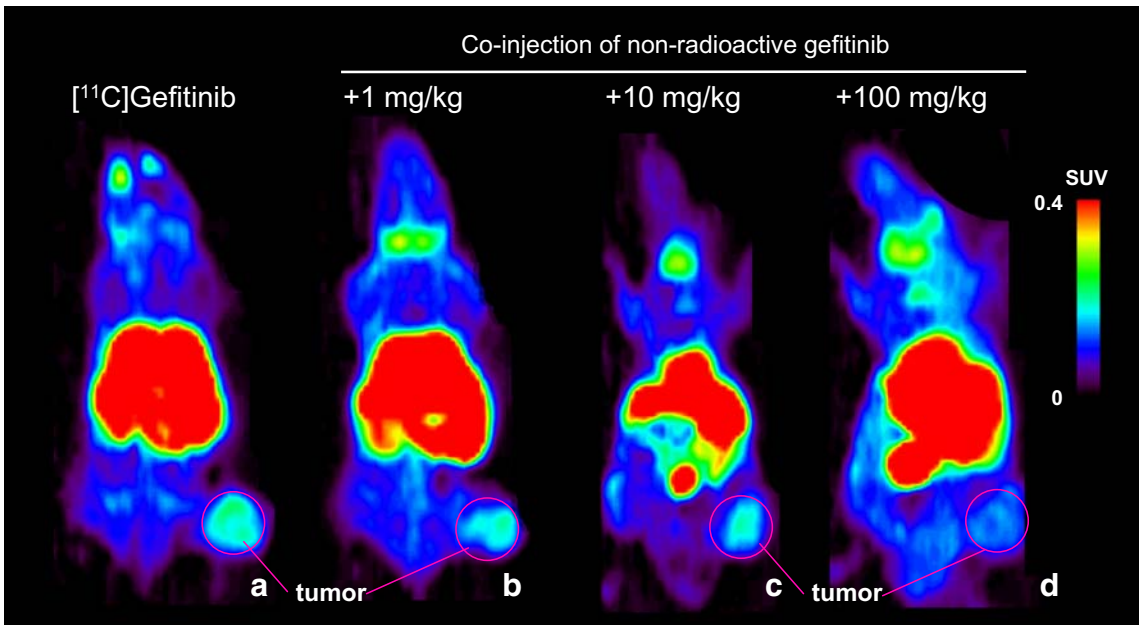

Fig. 7. PET summation images (30–60 min, transverse section) of the NFSa-bearing mice. **a** [^{11}C]Gefitinib only; **b** co-injection of [^{11}C]gefitinib with gefitinib of 1 mg/kg; **c** co-injection with gefitinib of 10 mg/kg; **d** co-injection with gefitinib of 100 mg/kg. By treating with gefitinib of 1, 10, and 100 mg/kg, the uptake of [^{11}C]gefitinib in the NFSa regions of same sizes was decreased to 78%, 66%, and 50% of the control, respectively.

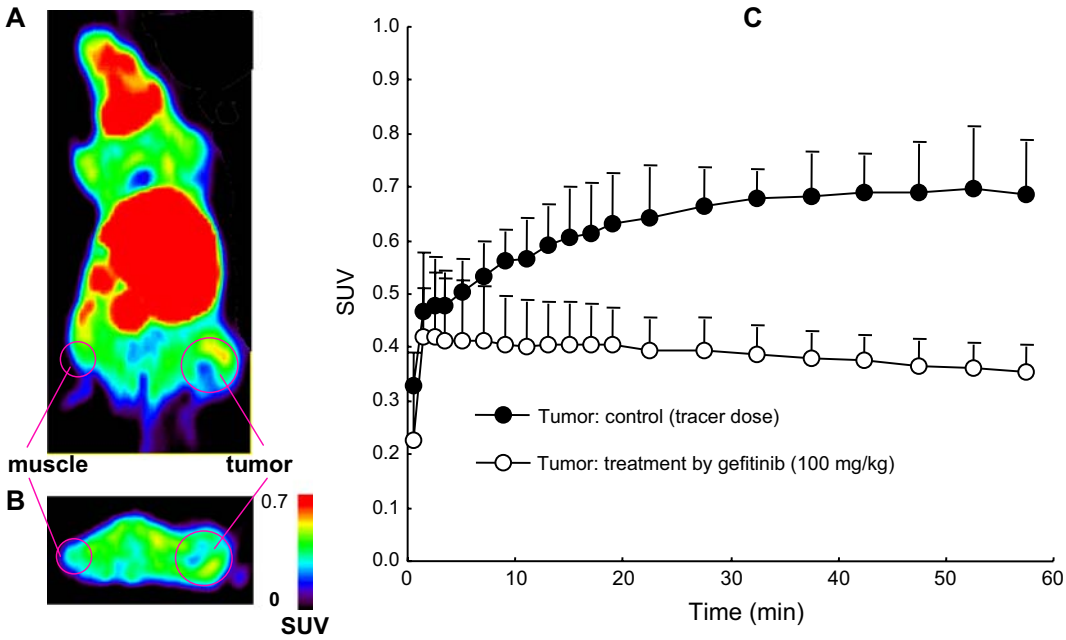

Fig. 8. Inhibitory effect of nonradioactive gefitinib (100 mg/kg) on [^{11}C]gefitinib PET. **a** Transverse section of PET summation image (0–60 min) after treatment with gefitinib; **b** coronary section by treatment; **c** comparison of TACs of tumors between control (*black dots*, $n=3$) and treatment groups (*circles*, $n=3$). By treatment with gefitinib, the difference of radioactivity between the tumor and muscle was almost abolished (**a**, **b**) and the control uptake was decreased to 50% at 60 min after injection (**c**).

We firstly demonstrated that [^{11}C]gefitinib is an *in vitro* specific ligand to NFSa cells (Fig. 3a). The uptake of [^{11}C]gefitinib into tumor cells was saturable during incubation. Competition with nonradioactive gefitinib decreased radioactivity uptake significantly, revealing that the uptake of [^{11}C]gefitinib was specific to this cell. To support the reliability of the present experimental protocol, we performed two similar *in vitro* experiments using EGFR/TK-rich A431 (Fig. 3b) and EGFR/TK-poor Jurkat (Fig. 3c) cells. A431 cells, a positive cell line with high expression of EGFR/TK, have been widely used to measure the inhibitory affinity of developed compounds for EGFR/TK [5]. As a negative control, EGFR/TK-poor Jurkat cells [5] were also used in these experiments. [^{11}C]Gefitinib had specific uptake to A431, like NFSa, but did not show specificity to Jurkat cells. The maximum uptake in NFSa cells (2.1 UR/mg protein) was slightly lower than that in A431 cells (2.6 UR/mg protein).

We further demonstrated that [^{11}C]gefitinib has *in vivo* specific binding in NFSa-bearing mice. [^{11}C]Gefitinib showed rapid penetration into the tumor even at 1 min after injection (Fig. 4). Radioactivity in the tumor increased over time and peaked (3.0–3.5% ID/g) between 30 and 60 min, whereas radioactivity in the blood and muscle as two comparative regions decreased slowly after rapid initial decline. The radioactivity ratios of tumor/muscle and tumor/blood reached the maximum levels at the end of this experiment (Fig. 5). This result indicated that [^{11}C]gefitinib could accumulate into the tumor specifically, which is a prerequisite as a promising PET ligand for tumor imaging.

PET images (Fig. 6) for NFSa-bearing mice were in agreement with the biodistribution data measured by the dissection method (Fig. 4). In addition to the high radioactivity level in the liver, kidney, and GI organs, a clear image of the tumor was obtained. Treatment by gefitinib of different doses reduced the uptake of [^{11}C]gefitinib in the tumor regions with a dose-dependent order (Fig. 7). In particular, co-injection with gefitinib (100 mg/kg) decreased the radioactivity ratio of tumor/muscle to near 1 and reduced the binding of [^{11}C]gefitinib in the tumor to 50% of the control (Fig. 8). Metabolite analysis revealed that the main radioactive component in the tumor homogenate was the intact [^{11}C]gefitinib. Thus, the high *in vivo* stability of this probe guaranteed that tumor imaging was not influenced by radioactive metabolites.

Despite high *in vitro* specific uptake to NFSa cells (>80% of the total uptake; Fig. 2a), the *in vivo* specific binding of [^{11}C]gefitinib comprised 50% of total binding (Fig. 8c) determined in NFSa-bearing mice. This reason may be considered from two aspects. The first is the weak inhibitory affinity of gefitinib to NFSa cells. Gefitinib was reported to have potent affinity for EGFR/TK (IC_{50}, 2 nM or 0.024–0.059 μM) and for various tumor cells (IC_{50}, 0.2–0.9 μM for human colon, breast, ovarian, and gastric cancer cells) [5–8]. In our experiment, gefitinib of 10 μM only reduced the uptake of [^{11}C]gefitinib at 60 min in NFSa and A431 cells to 69% and 54% of the control, respectively (Fig. 2). The low binding potency for NFSa cells may result in a high level of nonspecific binding in the tumor region. The second is the high lipophilicity (logP, 3.6) of [^{11}C]gefitinib. [^{11}C]Gefitinib was distributed throughout the body and displayed a slow decline of radioactivity from the main organs. Even in the muscle, a comparison region for the tumor, radioactivity decreased very slowly.

To increase the *in vivo* specific binding of gefitinib, chemical modification may be performed. Searching for compounds with more inhibitory affinity not only for purified EGFR/TK but also for tumor cells with a high expression and normal level of EGFR/TK is necessary. Medicinal chemists have constructed libraries containing a large number of potent gefitinib analogs [36–38]. When selecting a compound as an imaging probe from the library, the suitable lipophilicity of the candidates should be considered. Although low lipophilicity may reduce nonspecific binding *in vivo*, sufficient lipophilicity could guarantee high permeability of the probe through the cell membrane to reach action site inside the cell. On the other hand, from the radiochemistry point of view, labeling a ligand with a longer-lived radioactive isotope is an alternative method for reducing nonspecific binding. For example, labeling gefitinib analogs with longer-lived isotopes such as ^{124}I may give more specific PET image than using [^{11}C]gefitinib. Since washout of nonspecific binding from the target and comparative regions often requires time, long half-time of the positron-emitting radioactive isotope could make a long PET scan possible.

In this study, the *in vitro* experiment revealed that [^{11}C] gefitinib accumulated into EGFR/TK-rich A431 cells but did not accumulate into EGFR/TK-poor Jurkat cells (Fig. 2). Western blot analysis also identified the expression of EGFR in A431 cells and no EGFR expression in Jurkat cells (data not shown). This result supported that [^{11}C] gefitinib is a specific ligand binding with EGFR/TK. However, it has been reported that there was no significant difference of [^{18}F]gefitinib uptake between U87 xenografts (no EGFR expression) and U87-EGFR xenografts (overexpression of EGFR) [25]. The discrepancy of tumor uptakes between [^{11}C]gefitinib and [^{18}F] gefitinib may be due to the different types of tumor cell lines used in these experiments.

Despite the *in vitro* result on A431 and Jurkat cells, the tumor uptake of [^{11}C]gefitinib in A431 and Jurkat-bearing nude mice was similar and very low (data not shown). Moreover, in the PET images, both tumors showed no focal uptake when compared to surrounding skeletal muscle. The reason about the difference between *in vitro* and *in vivo* results was unclear. Similarly, low tumor uptake of [^{18}F] gefitinib was also detected in U87 xenografts and U87-EGFR xenograft-bearing mice [25]. On the other hand, using Western blot analysis techniques, we failed to confirm the presence of EGFR in NFSa cells. Therefore, the specific binding of [^{11}C]gefitinib in NFSa cells and NFSa-bearing mice may not be related to EGFR. Although we have not characterized the *in vivo* specific binding successfully, the present results have promoted us to determine whether [^{11}C] gefitinib PET could be used to evaluate the therapeutic effect of CIRT in the next study.

In conclusion, the present study demonstrated that [^{11}C] gefitinib is a promising PET probe for the imaging of NFSa-bearing mice.

Acknowledgments. We are grateful to Mrs. T. Igarashi, M. Takei, and I. Nakamura (Tokyo Nuclear Service Co., Ltd.) for technical support for radiosynthesis procedures. We also thank the staff of the Cyclotron Operation Section and Department of Molecular Probes, National Institute of Radiological Sciences (NIRS) for support for the cyclotron operation and animal experiments. This study was supported in part by a Grant-in-Aid for the Molecular Imaging Program from the Ministry of Education, Culture, Sports, Science and Technology, Japanese Government.

References

1. Khazaie K, Schirrmacher V, Lichtner RB (1993) EGF receptor in neoplasia and metastasis. Cancer Metastasis Rev 12:255–274
2. Voldborg BR, Damstrup L, Spang-Thomsen M, Poulsen HS (1997) Epidermal growth factor receptor (EGFR) and EGFR mutations, function and possible role in clinical trials. Ann Oncol 8:1197–1206
3. Boschelli DH (2002) 4-Anilino-3-quinolinecarbonitriles: an emerging class of kinase inhibitors. Curr Top Med Chem 2:1051–1063
4. Raymond E, Faivre S, Armand JP (2000) Epidermal growth factor receptor tyrosine kinase as a target for anticancer therapy. Drugs 60 (suppl 1):15–23
5. Ciardiello F, Caputo R, Bianco R et al (2001) Inhibition of growth factor production and angiogenesis in human cancer cells by ZD1839 (Iressa), a selective epidermal growth factor receptor tyrosine kinase inhibitor. Clin Cancer Res 7:1459–1465
6. Moulder SL, Yakes FM, Muthuswamy SK, Bianco R, Simpson JF, Arteaga CL (2001) Epidermal growth factor receptor (HER1) tyrosine kinase inhibitor ZD1839 (Iressa) inhibits HER2/*neu* (*erb*B2)-over-expressing breast cancer cells *in vitro* and *in vivo*. Cancer Res 61:8887–8895
7. Wakeling AE, Guy SP, Woodburn JR et al (2002) ZD1839 (Iressa): an orally active inhibitor of epidermal growth factor signaling with potential for cancer therapy. Cancer Res 62:5749–5754
8. Anido J, Matar P, Albanell J et al (2003) ZD1839, a specific epidermal growth factor receptor (EGFR) tyrosine kinase inhibitor, induces the formation of inactive EGFR/HER2 and EGFR/HER3 heterodimers and prevents heregulin signaling in HER2-overexpressing breast cancer cells. Clin Cancer Res 9:1274–1283
9. Bellomi M, Petralia G, Sonzogni A, Zampino MG, Rocca A (2007) CT perfusion for the monitoring of neoadjuvant chemotherapy and radiation therapy in rectal carcinoma: initial experience. Radiology 244:486–493
10. Søvik A, Kippenes SH, Bruland ØS, Rune OD, Malinen E (2008) DCEMRI monitoring of canine tumors during fractionated radiotherapy. Acta Oncol 47:1249–1256
11. Mikhaeel NG (2006) Use of FDG-PET to monitor response to chemotherapy and radiotherapy in patients with lymphomas. Eur J Nucl Med Mol Imaging 33(Suppl 1):22–26
12. Molthoff CF, Klabbers BM, Berkhof J et al (2007) Monitoring response to radiotherapy in human squamous cell cancer bearing nude mice: comparison of 2′-deoxy-2′-[18F]fluoro-D-glucose (FDG) and 3′-[18F] fluoro-3′-deoxythymidine (FLT). Mol Imaging Biol 9:340–347
13. Van de Wiele C, Lahorte C, Oyen W et al (2003) Nuclear medicine imaging to predict response to radiotherapy: a review. Int J Radiat Oncol Biol Phys 55:5–15
14. Riesterer O, Milas L, Ang KK (2007) Use of molecular biomarkers for predicting the response to radiotherapy with or without chemotherapy. J Clin Oncol 25:4075–4083
15. Fredriksson A, Stone-Elander S (2003) PET screening of anticancer drugs. A faster route to drug/target evaluations *in vivo*. Methods Mol Med 85:279–294
16. Bading JR, Shields AF (2008) Imaging of cell proliferation: status and prospects. J Nucl Med 49(Suppl 2):64S–80S
17. Ishikawa H, Tsuji H, Kamada T et al (2006) Risk factors of late rectal bleeding after carbon ion therapy for prostate cancer. Int J Radiat Oncol Biol Phys 66:1084–1091
18. Tsuji H, Mizoe J, Kamada T et al (2007) Clinical results of carbon ion radiotherapy at NIRS. J Radiat Res 48S:A1–A13
19. Sugane T, Baba M, Imai R et al (2009) Carbon ion radiotherapy for elderly patients 80 years and older with stage I non-small cell lung cancer. Lung Cancer 64:45–50
20. Zhang H, Yoshikawa K, Tamura K et al (2004) [^{11}C]Methionine positron emission tomography and survival in patients with bone and soft tissue sarcomas treated by carbon ion radiotherapy. Clin Cancer Res 10:1764–1772

21. Koizumi M, Saga T, Yoshikawa K et al (2008) ^{11}C-Methionine-PET for evaluation of carbon ion radiotherapy in patients with pelvic recurrence of rectal cancer. Mol Imaging Biol 10:374–380
22. Holt DP, Ravert HT, Dannals RF, Pomper MG (2006) Synthesis of [^{11}C]gefitinib for imaging epidermal growth factor receptor tyrosine kinase with positron emission tomography. J Labelled Comp Radiopharm 49:883–888
23. Wang JQ, Gao M, Miller KD, Sledge GW, Zheng QH (2006) Synthesis of [^{11}C]Iressa as a new potential PET cancer imaging agent for epidermal growth factor receptor tyrosine kinase. Bioorg Med Chem Lett 16:4102–4106
24. DeJesus OT, Murali D, Flores LG et al (2003) Synthesis of [^{18}F]-ZD1839 as a PET imaging agent for epidermal growth factors receptors. J Labelled Comp Radiopharm 46:s1
25. Su H, Seimbille Y, Ferl GZ et al (2008) Evaluation of [^{18}F]gefitinib as a molecular imaging probe for the assessment of the epidermal growth factor receptor status in malignant tumors. Eur J Nucl Med Mol Imaging 35:1089–1099
26. Ando K, Koike S, Fukuda N, Kanehira C (1984) Independent effect of a mixed-beam regimen of fast neutrons and gamma rays on a murine fibrosarcoma. Radiat Res 98:96–106
27. Ando K, Koike S, Ohira C et al (1999) Accelerated reoxygenation of a murine fibrosarcoma after carbon-ion radiation. Int J Radiat Biol 75:505–512
28. Koike S, Ando K, Oohira C et al (2002) Relative biological effectiveness of 290 MeV/u carbon ions for the growth delay of a radioresistant murine fibrosarcoma. J Radiat Res 43:247–255
29. Ando K, Koike S, Uzawa A et al (2005) Biological gain of carbon-ion radiotherapy for the early response of tumor growth delay and against early response of skin reaction in mice. J Radiat Res 46:51–57
30. Suzuki K, Inoue O, Hashimoto K, Yamasaki T, Kuchiki M, Tamate K (1985) Computer-controlled large scale production of high specific activity [11C]Ro 15–1788 for PET studies of benzodiazepine receptors. Int J Appl Radiat Isot 36:971–976
31. Takei M, Kida T, Suzuki K (2001) Sensitive measurement of positron emitters eluted from HPLC. Appl Radiat Isot 55:229–234
32. Elkind NB, Szentpetery Z, Apati A et al (2005) Multidrug transporter ABCG2 prevents tumor cell death induced by the epidermal growth factor receptor inhibitor Iressa (ZD1839, gefitinib). Cancer Res 65:1770–1777
33. Mishani E, Abourbeh G, Jacobson O et al (2005) High-affinity epidermal growth factor receptor (EGFR) irreversible inhibitors with diminished chemical reactivities as positron emission tomography (PET)-imaging agent candidates of EGFR overexpressing tumors. J Med Chem 48:5337–5348
34. Pal A, Glekas A, Doubrovin M et al (2006) Molecular imaging of EGFR kinase activity in tumors with 124I-labeled small molecular tracer and positron emission tomography. Mol Imaging Biol 8:262–277
35. Mishani E, Abourbeh G (2007) Cancer molecular imaging: radionuclide-based biomarkers of the epidermal growth factor receptor (EGFR). Curr Top Med Chem 7:1755–1772
36. Ghosh S, Liu XP, Zheng Y, Uckun FM (2001) Rational design of potent and selective EGFR tyrosine kinase inhibitors as anticancer agents. Curr Cancer Drug Targets 1:129–140
37. Bianco R, Damiano V, Gelardi T, Daniele G, Ciardiello F, Tortora G (2007) Rational combination of targeted therapies as a strategy to overcome the mechanisms of resistance to inhibitors of EGFR signaling. Curr Pharm Des 13:3358–3367
38. Press MF, Lenz HJ (2007) EGFR, HER2 and VEGF pathways: validated targets for cancer treatment. Drugs 67:2045–2075